

Review of Inverse Laplace Transform Algorithms for Laplace-Space

Numerical Approaches

Kristopher L. Kuhlman

the date of receipt and acceptance should be inserted later

Abstract A boundary element method (BEM) simulation is used to compare the efficiency of numerical inverse Laplace transform strategies, considering general requirements of Laplace-space numerical approaches. The two-dimensional BEM solution is used to solve the Laplace-transformed diffusion equation, producing a time-domain solution after a numerical Laplace transform inversion. Motivated by the needs of numerical methods posed in Laplace-transformed space, we compare five inverse Laplace transform algorithms and discuss implementation techniques to minimize the number of Laplace-space function evaluations. We investigate the ability to calculate a sequence of time domain values using the fewest Laplace-space model evaluations. We find Fourier-series based inversion algorithms work for common time behaviors, are the most robust with respect to free parameters, and allow for straightforward image function evaluation re-use across at least a log cycle of time.

Keywords numerical Laplace transform inversion · boundary element method · 2D diffusion · Helmholtz equation · Laplace-space numerical methods · groundwater modeling

1 Introduction

Simulation methods that are posed in Laplace-transformed space, then numerically inverted back to the time domain (i.e., Laplace-space methods), are a viable alternative to the more standard use of finite

Repository Performance Department, Sandia National Laboratories

4100 National Parks Highway, Carlsbad, New Mexico, USA

Tel: +1 575-234-0084

E-mail: kkuhlm@sandia.gov

4 differences in time. We use the the two-dimensional boundary element method (BEM) as an example of
5 this type of approach, to solve the Laplace-transformed diffusion equation (i.e., the Yukawa or modified
6 Helmholtz equation). We investigate five numerical inverse Laplace transform methods and implementa-
7 tion approaches, namely the methods of [Stehfest(1970)], [Schapery(1962)], [Weeks(1966)], [Talbot(1979)],
8 and [de Hoog et al(1982)]. Naively implemented Laplace-space simulations can be more computationally
9 expensive than using finite differences in time, but they have the advantage of allowing evaluation at
10 any time, without evolving from an initial condition, and image function calculations are trivially par-
11 allelized across Laplace parameters [Davies and Crann(2002)]. When Laplace-space numerical models are
12 used in parameter estimation, hundreds or thousands of forward simulations may be required – making
13 forward model efficiency critical. Although parameter estimation may be done directly in Laplace space
14 [Barnhart and Illangasekare(2012)], choosing an efficient inversion strategy is important in most applica-
15 tions.

16 The Laplace transform has a long history of use to derive analytical solutions to diffusion and wave
17 problems (e.g., see list of citations by [Duffy(2004), pp. 191-220]). Often the analytical inverse trans-
18 form is too difficult to find or evaluate in closed form. A researcher then resorts to approximate ana-
19 lytical methods (e.g., [Hantush(1960), Sternberg(1969)]) or numerical inversion (e.g., [Malama et al(2009),
20 Mishra and Neuman(2010)]). Numerical methods can similarly benefit from the Laplace transform, convert-
21 ing the time-dependence of a differential equation to parameter dependence. Laplace-space finite-element
22 approaches have seen application to groundwater flow and solute transport (e.g., [Sudicky and McLaren(1992),
23 Morales-Casique and Neuman(2009)]), and Laplace-space BEM has also been used in groundwater applica-
24 tions (e.g., [Kythe(1995), §10.3] or [Liggett and Liu(1982), §10.1]). The Laplace transform analytic element
25 method [Kuhlman and Neuman(2009)] is a transient extension of the analytic element method. These dif-
26 ferent Laplace-space approaches may have diverse spatial solution strategies, but they have a common
27 requirement of effective Laplace transform numerical inversion algorithms. We couple a BEM model in the
28 Laplace domain with a numerical Laplace transform inversion routine, but our conclusions should be valid
29 for both gridded and mesh-free Laplace-space numerical methods. Any Laplace-space numerical approach
30 begins with determination of optimal Laplace parameter values. Then each image function evaluation is
31 computed from the simulation. The final step involves approximating the time-domain solution from the
32 vector of image function values using the algorithm of choice.

33 [Bellman et al(1966)] was an early review book on numerical Laplace transform inversion for linear
34 and non-linear problems, but without the benefit of the many algorithms that have since been devel-
35 oped. [Davies and Martin(1979)] performed a thorough survey, assessing numerical Laplace transform in-
36 version algorithm accuracy for techniques available in 1979, using simple functions for their benchmarks.
37 [Duffy(1993)] reviewed the numerical inversion characteristics for more pathological time behaviors using
38 the Fourier series, Talbot, and Weeks inversion methods. The review book by [Cohen(2007)] summarizes
39 historical reviews and discusses commonly used inversion their variations. More details and examples can
40 be found in these reference regarding the convergence behavior of the five inversion algorithms discussed
41 here.

42 While these published numerical inverse Laplace transform algorithm reviews are thorough and useful,
43 they focus on computing a single time-domain solution as accurately as possible. These reviews did not try
44 to minimize Laplace-space function evaluations, since their functions were simple closed-form expressions,
45 not simulations. We investigate Laplace transform inversions algorithms that can compute a sequence of
46 time domain values using the fewest Laplace-space model evaluations possible, a desirable property for use
47 in Laplace-space numerical methods. Using numerical Laplace transform inversion in a simulation approach,
48 rather than a time-marching method, allows the researcher to readily switch between fast and accurate by
49 changing the number of approximation terms in the inversion.

50 In the next section we define the mathematical formulation of the governing equation and Laplace
51 transform. In the third section we introduce the five inverse Laplace transform algorithms. In the final
52 section we compare results using five different inversion algorithms to invert the BEM modified Helmholtz
53 solution on the same domain with four different boundary conditions, leading to recommendations for
54 Laplace-space numerical approaches.

55 **2 Governing Equation and Laplace Transform**

56 The BEM model generally simulates *substance* flow (e.g., energy or groundwater), which can be related to
57 a potential ϕ (e.g., temperature or hydraulic head). The medium property α is diffusivity [L^2/T], the ratio
58 of the conductance in the substance flux and potential gradient relation (e.g., Fourier's or Darcy's law)
59 to the substance capacity per unit mass (e.g., heat capacity or storativity). The BEM (e.g., [Kythe(1995)],

60 Liggett and Liu(1982),Brebba et al(1984)]) can be used to solve the diffusion equation

$$\nabla^2 \phi = \frac{1}{\alpha} \frac{\partial \phi}{\partial t}, \quad (1)$$

61 where α is a real constant in space and time. We consider (1) in a domain subject to a combination of
 62 Dirichlet $\phi(\Gamma_u(s), t) = f_u(s, t)$ and Neumann $\hat{n} \cdot \nabla \phi(\Gamma_q(s), t) = f_q(s, t)$ boundary conditions along the
 63 perimeter of the 2D domain $\Gamma = \Gamma_u \cup \Gamma_q$, where \hat{n} is the boundary unit normal, and s is a boundary
 64 arc-length parameter. Without loss of generality, we only consider homogeneous initial conditions.

65 The Laplace transform is

$$\mathcal{L}\{f(t)\} \equiv \bar{f}(p) = \int_0^\infty f(t)e^{-pt} dt, \quad (2)$$

66 where p is the generally complex-valued Laplace parameter, and the over-bar denotes a transformed variable.
 67 The transformed diffusion equation with zero initial conditions is the homogeneous Yukawa or modified
 68 Helmholtz equation,

$$\nabla^2 \bar{\phi} - q^2 \bar{\phi} = 0, \quad (3)$$

69 where $q^2 = p/\alpha$. Equation 3 arises in several groundwater applications, including transient, leaky, and lin-
 70 earized unsaturated flow [Bakker and Kuhlman(2011)]. The transformed boundary conditions are $\bar{\phi}(\Gamma_u(s)) =$
 71 $f_u(s)\bar{f}_t(p)$ and $\hat{n} \cdot \nabla \bar{\phi}(\Gamma_q(s)) = f_q(s)\bar{f}_t(p)$, where the temporal and spatial behaviors have been decomposed
 72 as in separation of variables. Arbitrary time behavior can be developed through convolution in t (Duhamel's
 73 theorem), which is multiplication of image functions in Laplace space. Here, $\bar{f}_t(p)$ represents the Laplace
 74 transform of the time behavior applied to the boundary conditions. The Laplace transformation makes it
 75 possible to solve transient diffusion (a parabolic equation) using the BEM, which is well-suited for elliptical-
 76 type equations.

77 The inverse Laplace transform is defined as the Bromwich contour integral,

$$\mathcal{L}^{-1}\{\bar{f}(p)\} = f(t) = \frac{1}{2\pi i} \int_{\sigma-i\infty}^{\sigma+i\infty} \bar{f}(p)e^{pt} dp, \quad (4)$$

78 where the abscissa of convergence $\sigma > 0$ is a real constant chosen to put the contour to the right of all
 79 singularities in $\bar{f}(p)$. In Laplace-space numerical approaches, (3) is solved by a suitable numerical method,
 80 therefore only samples of $\bar{f}(p)$ are available; this precludes an analytical inversion. Five numerical inverse
 81 Laplace transform algorithms are discussed in the following section.

82 **3 Numerical Inverse Laplace Transform Methods**

83 Equation 4 is an integral equation for unknown $f(t)$ given $\bar{f}(p)$; its numerical solution is broadly split into
 84 two categories. Methods are either based on quadrature or functional expansion using analytically invertible
 85 basis functions. [Davies(2005), Chap. 19] relates most major classes of inverse Laplace transform methods
 86 using a unified theoretical foundation; we adopt a simplified form of their general notation. The Fourier
 87 series and Talbot methods are quadrature-based, directly approximating (4). Weeks' and Piessen's methods
 88 are $\bar{f}(p)$ expansions using complex-valued basis functions, while the Gaver-Stehfest and Schapery methods
 89 use real-valued functions to accomplish this.

90 The numerical inverse Laplace transform is in general an ill-posed problem (e.g., [Al-Shuaibi(2001)]).
 91 No single approach is optimal for all circumstances and temporal behaviors, leading to the diversity of
 92 viable numerical approaches in the literature (e.g., [Cohen(2007)]).

93 **3.1 Gaver-Stehfest Method**

94 The Post-Widder formula [Widder(1941), Al-Shuaibi(2001)] is an approximation to (4) that only requires
 95 $\bar{f}(p)$ for real p to represent (2) as an asymptotic Taylor series expansion. The formula requires high-order
 96 analytic image function derivatives, and is impractical for numerical computation. Stehfest proposed a
 97 discrete version of the Post-Widder formula using finite differences and Salzer summation [Stehfest(1970)],

$$f(t, N) = \frac{\ln 2}{t} \sum_{k=1}^N V_k \bar{f}\left(k \frac{\ln 2}{t}\right). \quad (5)$$

98 The V_k coefficients only depend on the number of expansion terms, N (which must be even), which are

$$V_k = (-1)^{k+N/2} \sum_{j=\lfloor (k+1)/2 \rfloor}^{\min(k, N/2)} \frac{j^{\frac{N}{2}} (2j)!}{\left(\frac{N}{2} - j\right)! j! (j-1)! (k-j)! (2j-k)!}. \quad (6)$$

99 These become very large and alternate in sign for increasing k . The sum (5) begins to suffer from cancellation
 100 for $N \geq$ the number of decimal digits of precision (e.g., double precision = 16). For $\bar{f}_t(p)$ that are non-
 101 oscillatory and continuous, $N \leq 18$ is usually sufficient [Stehfest(1970)]. If programmed using arbitrary
 102 precision (e.g. Mathematica or a multi-precision library [Bailey et al(2002), Johansson(2011)]), the method
 103 can be made accurate for most cases [Abate and Valkó(2004)]. Unfortunately, p is explicitly a function of
 104 t ; for each new t , a new $\bar{f}(p)$ vector is needed. In Laplace-space numerical approaches, each vector element
 105 is constructed using a simulation, therefore this can be a large penalty.

106 The method is quite easy to program; the V_j can be computed once and saved as constants. This method
 107 has been popular due to its simplicity and adequacy for exponentially decaying $\bar{f}_t(p)$.

108 3.2 Schapery's Method

109 We can expand the deviation of $f(t)$ from steady-state f_s using exponential basis functions [Schapery(1962)],

$$f(t, N) = f_s + \sum_{i=1}^N a_i e^{-p_i t}, \quad (7)$$

110 where a_i is a vector of unknown constants. Applying (2) to (7) gives

$$\bar{f}(p_j, N) = \frac{f_s}{p_j} + \sum_{i=1}^N \frac{a_i}{p_i + p_j} \quad j = 1, 2, \dots, M. \quad (8)$$

111 The p_j are selected (a geometric series is recommended [Liggett and Liu(1982)]) to cover the important
 112 fluctuations in $\bar{f}(p)$. After setting $p_i = p_j$ the a_i coefficients can be determined as the solution to $P_{ij}a_i =$
 113 $(\bar{f}(p_j) - f_s/p_j)$. The symmetric matrix to decompose is

$$P_{ij} = \begin{bmatrix} (2p_1)^{-1} & (p_1 + p_2)^{-1} & \dots & (p_1 + p_N)^{-1} \\ (p_2 + p_1)^{-1} & (2p_2)^{-1} & \dots & (p_2 + p_N)^{-1} \\ \vdots & \vdots & \ddots & \vdots \\ (p_N + p_1)^{-1} & (p_N + p_2)^{-1} & \dots & (2p_N)^{-1} \end{bmatrix},$$

114 which only depends on p_j ; it can be decomposed independently of $\bar{f}(p)$ and f_s .

115 This method is not difficult to implement when existing matrix decomposition libraries are available, and
 116 only requires real computation. The method has been used for inverting BEM results [Liggett and Liu(1982)],
 117 but has two main drawbacks. First, in its formulation above, it requires a steady-state solution, but (7)
 118 could be posed without f_s . Secondly, no theory is presented for optimally picking p_j ; some trial and error
 119 is required [Liggett and Liu(1982)].

120 3.3 Möbius Transformation Methods

121 We can use the Möbius transformation to conformally map the half-plane right of σ to the unit disc, mak-
 122 ing the Laplace domain more amenable to approximation using orthonormal polynomials (e.g., Chebyshev
 123 [Piessens(1972)], [Lanczos(1988), §28] or Laguerre [Weeks(1966)], [Lyness and Giunta(1986)], [Lanczos(1988),
 124 §30]). If σ was chosen properly, $\bar{f}(p)$ is guaranteed to be analytic inside the unit circle. The most-used inverse

125 Laplace transform method from this class is Weeks' method, which uses a complex power series to expand
 126 $\bar{f}(p)$ inside the unit circle. Upon inverse Laplace transformation, the power series becomes a Laguerre
 127 polynomial series.

128 Weeks method is

$$f(t, N + 1) = e^{(\kappa - b/2)t} \sum_{n=0}^N a_n L_n(bt), \quad (9)$$

129 where $L_n(z)$ is an n -order Laguerre polynomial and κ and b are free parameters. Weeks suggested $\kappa =$
 130 $\sigma + 1/t_{\max}$ and $b = N/t_{\max}$, where t_{\max} is the maximum transformed time. The parameters b and κ are
 131 chosen to optimize convergence; some schemes are given [Weideman(1999)] for finding optimum parameter
 132 values for a given $\bar{f}_t(p)$, but search techniques require hundreds of $\bar{f}(p)$ evaluations. A more general form of
 133 (9) can also be used, which allows for more general asymptotic behavior of the image function [Davies(2005),
 134 §19.5]. Weeks assumed $p\bar{f}(p)$ is analytic at infinity. The Laplace transform of (9) is known, but to make it
 135 easier to represent with polynomials, $\bar{f}(p)$ is mapped inside the unit circle via $z = (p - \kappa - 2b)/(p - \kappa + 2b)$.
 136 The coefficients a_n are determined by the midpoint rule,

$$a_n = \frac{1}{2M} \sum_{j=-M}^{M-1} \Psi \left[\exp \left(i\theta_{j-\frac{1}{2}} \right) \right] \exp \left(-in\theta_{j-\frac{1}{2}} \right) \quad (10)$$

137 where $\theta_j = j\pi/M$ and the conformally-mapped image function is

$$\Psi(z) = \frac{b}{1-z} \bar{f} \left(\kappa - \frac{b}{2} + \frac{b}{1-z} \right). \quad (11)$$

138 The argument of $\bar{f}(z)$ in (11) is the inverse mapping of $z \mapsto p$, it shows p does not functionally depend on
 139 t , but Weeks' rules-of-thumb for b and κ depend on t_{\max} .

140 There are other related methods which use different orthonormal polynomials to represent $\bar{f}(p)$ inside
 141 the unit circle. Chebyshev polynomials (known as Piessen's method [Piessens(1972)]) can be used to expand
 142 the $\bar{f}(z)$ on the real interval $[-1, 1]$. The Weeks method is moderately easy to program, requiring the use
 143 of Clenshaw recurrence formula to accurately implement Laguerre polynomials. Piessen's method is similar
 144 to implement, with a similar recurrence formula for Chebyshev polynomials.

145 3.4 Talbot Method

146 We can deform the Bromwich contour into a parabola around the negative real axis if $\bar{f}(p)$ is analytic
 147 in the region between the Bromwich and the deformed Talbot contours [Talbot(1979)]. Numerically, $\bar{f}(p)$

148 must not overflow as $p \rightarrow -\infty$ (e.g., in the BEM implementation, the Green's function is the second-kind
 149 modified Bessel function, which grows exponentially as $p \rightarrow -\infty$). Oscillatory $\bar{f}_t(p)$ often have pairs of poles
 150 near the imaginary p axis; these poles must remain to the left of the deformed contour.

151 The Talbot method makes the Bromwich contour integral converge rapidly, since p becomes large and
 152 negative, making the e^{pt} term in (4) very small. A one-parameter "fixed" Talbot method was implemented
 153 [Abate and Valkó(2004)]; the Bromwich contour is parametrized as $p(\theta) = r\theta(\cot(\theta) + i)$, where $0 \leq \theta \leq \pi$,
 154 and as a rule of thumb $r = 2M/(5t_{\max})$. The fixed Talbot method is

$$f(t, N) = \frac{r}{N} \left[\frac{\bar{f}(r)}{2} e^{rt} + \sum_{k=1}^{N-1} \Re \left\{ e^{tp(\theta_k)} \bar{f}[p(\theta_k)] [1 + i\zeta(\theta_k)] \right\} \right], \quad (12)$$

155 where $\zeta(\theta_k) = \theta_k + [\theta_k \cot(\theta_k) - 1] \cot(\theta_k)$ and $\theta_k = k\pi/N$ [Abate and Valkó(2004)]. Although $\bar{f}(p)$ doesn't
 156 depend on t , the free parameter r depends on t_{\max} .

157 Step change $\bar{f}_t(p)$ for non-zero time become very large as $p \rightarrow -\infty$, since $\mathcal{L}[H(t - \tau)] = e^{-\tau p}/p$, where
 158 $H(t - \tau)$ is the Heaviside step function centered on time τ . This can lead to precision loss, and stability
 159 or convergence issues with the underlying numerical model, although Mathematica's arbitrary precision
 160 capabilities have been used to get around this problem [Abate and Valkó(2004)].

161 The fixed Talbot method is very simple to program; [Abate and Valkó(2004)] provide a ten-line Math-
 162 ematica implementation.

163 3.5 Fourier Series Method

164 We can manipulate (4) into a Fourier transform; first it is expanded into real and imaginary parts ($p =$
 165 $\gamma + i\omega$),

$$f(t) = \frac{e^{\gamma t}}{2\pi i} \int_{-\infty}^{\infty} [\cos(\omega t) + i \sin(\omega t)] \{ \Re [\bar{f}(p)] + i \Im [\bar{f}(p)] \} i d\omega.$$

166 Multiplying out the terms, keeping only the real part due to $f(t)$ symmetry, and halving the integration
 167 range due to symmetry again, leaves

$$f(t) = \frac{e^{\gamma t}}{\pi} \int_0^{\infty} \Re [\bar{f}(p)] \cos(\omega t) - \Im [\bar{f}(p)] \sin(\omega t) d\omega. \quad (13)$$

168 When $f(t)$ is real, (13) can be represented using the complex form or just its real or imaginary parts.

169 Although these three representations are equivalent, when evaluating (13) with the trapezoid rule, the full

170 complex form gives the smallest discretization error [Davies(2005)]. The trapezoid rule approximation to
 171 (13) is essentially a discrete Fourier transform,

$$f(t, 2N + 1) = \frac{e^{\gamma t}}{T} \sum_{k=0}^{2N}{}' \Re \left[\bar{f} \left(\gamma_0 + \frac{i\pi k}{T} \right) \exp \left(\frac{i\pi k t}{T} \right) \right], \quad (14)$$

172 where $\gamma_0 = \sigma - \log(\epsilon)/T$, ϵ is the desired relative accuracy (typically 10^{-8} in double precision), T is a scaling
 173 parameter (often $2t_{\max}$), and the prime indicates the $k = 0$ summation term is halved. The p in (14) do
 174 not depend on t , but the free parameter T depends on t_{\max} .

175 The non-accelerated Fourier series inverse algorithm 14 is almost useless because it requires thousands
 176 of $\bar{f}(p)$ evaluations [Antia(2002), §9.8]. Practical approaches accelerate the convergence of the sum in 14.
 177 Although this is sometimes called a fast-Fourier transform (FFT) method (e.g., [Cohen(2007), Chap 4.4]),
 178 rarely do the number of $\bar{f}(p)$ evaluations in an accelerated approach justify an FFT approach. The method
 179 implemented uses non-linear double acceleration with Padé approximation and an analytic expression for
 180 the remainder in the series [de Hoog et al(1982)]. Although there are several other ways to accelerate the
 181 Fourier series approach [Cohen(2007)], this method is popular and straightforward. Non-linear acceleration
 182 techniques drastically reduce the required number of function evaluations, but can lead to numerical dis-
 183 persion [Kano et al(2005), Morales-Casique and Neuman(2009)]. For diffusion, dispersion associated with
 184 non-linear acceleration is not noticeable. Schapery's, Talbot's, and Weeks' methods are not accelerated in
 185 a non-linear manner, and therefore may lead to less numerical dispersion, which may be more important
 186 in wave systems with sharp fronts.

187 The creation of the Padé approximation [de Hoog et al(1982)] is relatively straightforward in program-
 188 ming languages that facilitate matrix manipulations (e.g., modern Fortran, Matlab, or NumPy [Oliphant(2007)]).
 189 There is no dependence on matrix decomposition routines.

190 3.6 Algorithm Properties Summary

191 Table 1 summarizes aspects of the five inverse methods. The third column indicates whether p is explicitly
 192 a function of t , the fourth column indicates if the rules-of-thumb used for the optimum parameters depend
 193 on t_{\max} , and the fifth column indicates whether the transform requires complex p and $\bar{f}(p)$.

194 For all methods considered here, computational effort to compute $f(t)$ from the vector of $\bar{f}(p)$ values
 195 was insignificant compared to the effort required to compute the BEM solution used to fill the $\bar{f}(p)$ vector.

Table 1 Algorithmic Summary

Method	Limitations on $\bar{f}(p)$ and $f(t)$	$p(t)$?	$p(t_{\max})$?	p
Stehfest	no oscillations, no discontinuities in $f(t)$	yes	no	real
Schaperly	smoothly varying $f(t)$, f_s exists	no	no	real
Weeks	none	no	yes	complex
fixed Talbot	no high-frequency $f(t)$, $\bar{f}(p \rightarrow -\infty)$ exists	no	yes	complex
Fourier series	none	no	yes	complex

196 This suggests a more complicated method, which allows re-use of $\bar{f}(p)$ across more values of t and converges
 197 in less evaluations of $\bar{f}(p)$, would be efficient for Laplace-domain numerical methods. If existing libraries
 198 or simulations only support real arguments, then the Stehfest, Schaperly, or Piessen’s methods must be
 199 used. Complex p methods will pay a slight penalty in computational overhead compared to real-only p
 200 routines. Computing with arbitrary or higher-than-double precision (e.g., [Abate and Valkó(2004)]) will
 201 incur a much larger penalty than the change from real to complex double precision. Generally, complex
 202 p methods have better convergence properties than real-only methods. Expansion of $\bar{f}(p)$ along the real p
 203 axis is separation of non-orthogonal exponentials, while expansion along the imaginary p axis is separation
 204 of oscillatory functions [Lanczos(1988), §29].

205 **4 Numerical Comparison**

206 Four test problems were solved using the BEM for values of p required by each algorithm’s rules of thumb.
 207 The test problem domain is a 3×2 rectangle, with homogeneous initial conditions and specified potential
 208 at two ends $\bar{\phi}(x = 0) = -2\bar{f}_t(p)$, and $\bar{\phi}(x = 3) = 2\bar{f}_t(p)$, and zero normal flux along the other sides
 209 $\partial\bar{\phi}/\partial y(y = \{0, 2\}) = 0$. All plots show the solution computed at a point closer to the $x = 0$ boundary
 210 ($x = 1/3$), midway between the insulated boundaries ($y = 1$).

211 The first problem computes $\bar{f}(p)$ using the optimum p at each t (like most inverse Laplace transform
 212 surveys), according to the rules-of-thumb for each method. While this is most accurate, it is very inefficient
 213 – especially when many values of t are required. In the following sections, all methods except Stehfest
 214 use the same $\bar{f}(p)$ to invert all t . A method’s sensitivity to non-optimal free parameters is important in
 215 practical use for Laplace-space numerical approaches. By inverting more than one time with the same set
 216 of Laplace-space function evaluations, large gains in efficiency can be made. The t range used in the plots

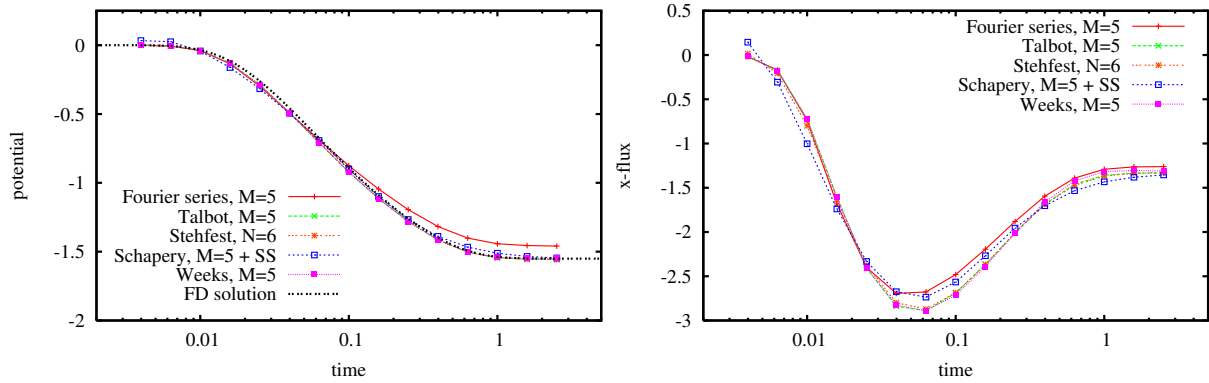


Fig. 1 Plots of potential and flux through time with five methods for $\bar{f}_t(p) = 1/p$, using optimum p at each t . $15 \times 5 = 75$ total $\bar{f}(p)$ evaluations are used by each method.

217 spans three orders of magnitude; it was chosen to show the evolution of potential and substance flux from
 218 initial conditions to steady state.

219 4.1 Steady Boundary Conditions, Optimum p

220 The first problem has steady-state boundary conditions. The transient behavior is solely due to evolution
 221 from the zero initial condition, $\bar{f}_t(p) = \mathcal{L}[H(t)] = 1/p$; $\bar{f}(p)$ has a pole at the origin. All methods performed
 222 equally well with this simple test problem, although the Fourier series method deviates from the finite
 223 difference solutions at larger time. Figure 1 shows the inverted potential and flux using as few evaluations
 224 of $\bar{f}(p)$ possible, without major deviations from the finite difference benchmark solution. Some trial and
 225 error was needed to use the Schapery method (i.e., further optimization may be possible).

226 As shown in Figure 2, all the methods performed very well for nine $\bar{f}(p)$ terms per t but at least 135 $\bar{f}(p)$
 227 evaluations are needed total for each method. Schapery's method does the worst in this case, but this may
 228 be improved with further optimization of p_j values. The finite-difference approach took at least an order
 229 of magnitude less computational effort for the given accuracy. Making Laplace-space numerical methods
 230 useful alternatives to traditional time-marching approaches, requires improvements to this inefficiency.

231 4.2 Steady Boundary Conditions, Same p

232 All methods had more difficulty obtaining accurate results for a wide t range using only one vector of $\bar{f}(p)$
 233 (no Stehfest method, since p explicitly depends on t). Only the last log-cycle of times is inverted accurately
 234 when using nine $\bar{f}(p)$ (Figure 3). All the methods – except possibly Schapery's – have a more difficult

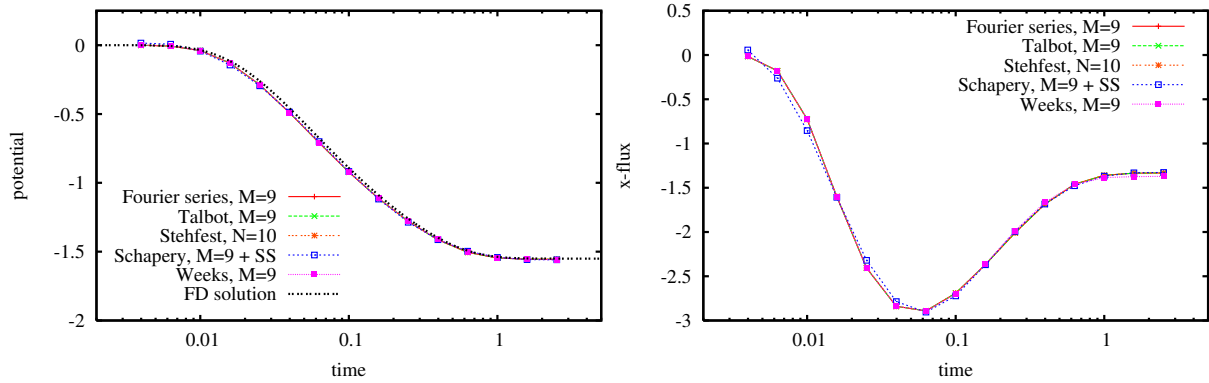


Fig. 2 Plots of potential and flux through time with five methods for $\bar{f}_t(p) = 1/p$, using optimum p at each t . $15 \times 9 = 135$ total $\bar{f}(p)$ evaluations are used by each method. Fourier series, Talbot, Stehfest, and Weeks curves are nearly coincident.

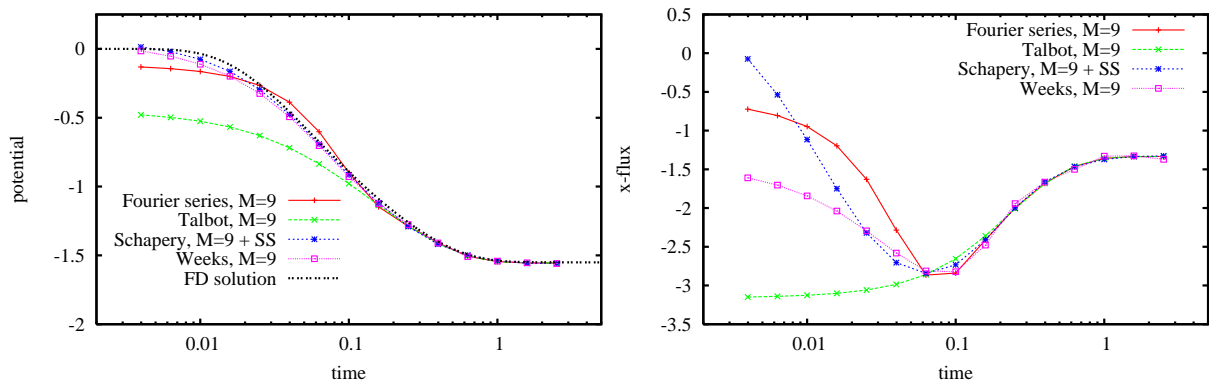


Fig. 3 Plots of potential and flux through time with four methods for $\bar{f}_t(p) = 1/p$, same p used across all t . Nine total $\bar{f}(p)$ evaluations are used by each method.

235 time with the flux at early time (especially the fixed Talbot method). The apparent success of Schapery's
 236 method can be attributed to the expansion of the deviation from steady-state, which in this case decays
 237 exponentially with time.

238 Figure 4 shows that when increasing to 51 $\bar{f}(p)$ terms, most convergence problems disappear, except
 239 at small times. Grouping t values by log-cycles and inverting them together using the same $\bar{f}(p)$ is more
 240 economical than using the optimal p for each t and is still relatively accurate. The results shown in Figure 4
 241 are nearly as accurate as those shown in Figure 2, but required $1/3$ the $\bar{f}(p)$ model evaluations.

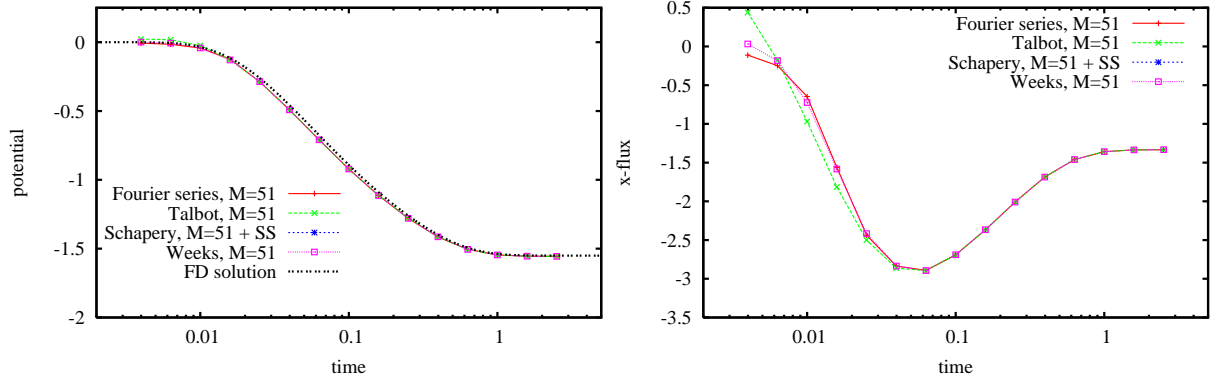


Fig. 4 Plots of potential and flux through time with four methods for $\bar{f}_t(p) = 1/p$, same p used across all t . 51 total $\bar{f}(p)$ evaluations used by each method. Schapery and Weeks curves are nearly coincident.

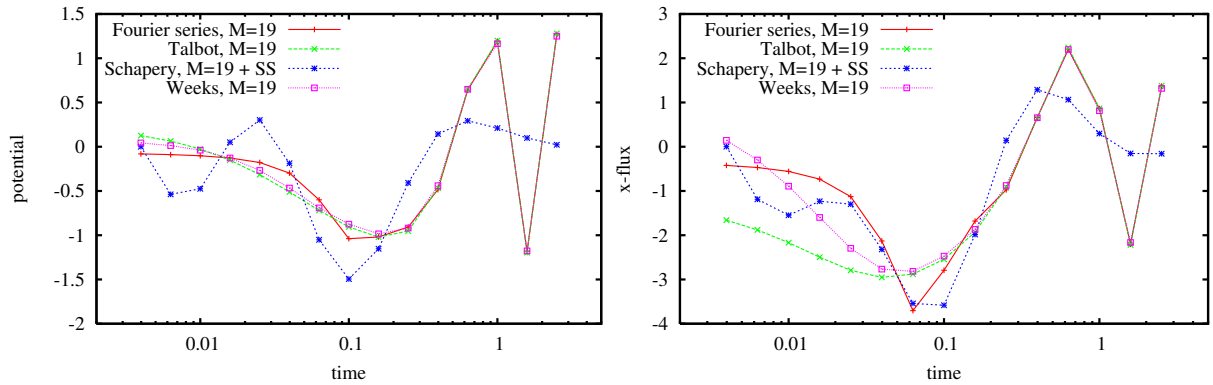


Fig. 5 Plots of potential and flux through time with four methods for $\bar{f}_t(p) = p/(p^2 + 16)$, same p used across all t . 19 total $\bar{f}(p)$ evaluations are used by each method.

242 4.3 Sinusoidal Boundary Conditions, Same p

243 This problem uses temporally sinusoidal boundary conditions, $\bar{f}_t(p) = \mathcal{L}(\cos 4t) = \frac{p}{p^2 + 16}$. This boundary
 244 condition violates some assumptions of the inverse transform algorithms (i.e., no steady-state solution,
 245 oscillatory in time), but the behavior is still relatively simple and smooth, with singularities at $p = \pm 4i$.

246 Figure 5 shows the Schapery method fails since there is no f_s , but the other methods do well for 19
 247 terms across one t log cycle. Figure 6 shows all methods besides Schapery do well for 51 terms, across
 248 at least two t log cycles. A modified version of (8) substituting $\frac{p_j}{p_j^2 + 16}$ for f_s/p_j could extend Schapery's
 249 approach to this case, but this solution was not considered here because of its problem specificity.

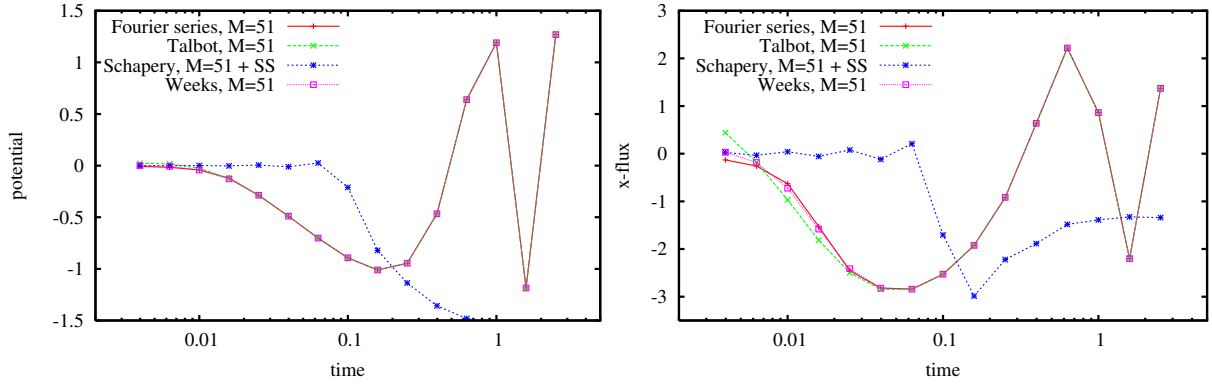


Fig. 6 Plots of potential and flux through time with four methods for $\bar{f}_t(p) = p/(p^2 + 16)$, same p used across all t . 51 total $\bar{f}(p)$ evaluations are used by each method. Fourier series, Talbot, and Weeks curves are nearly coincident for potential.

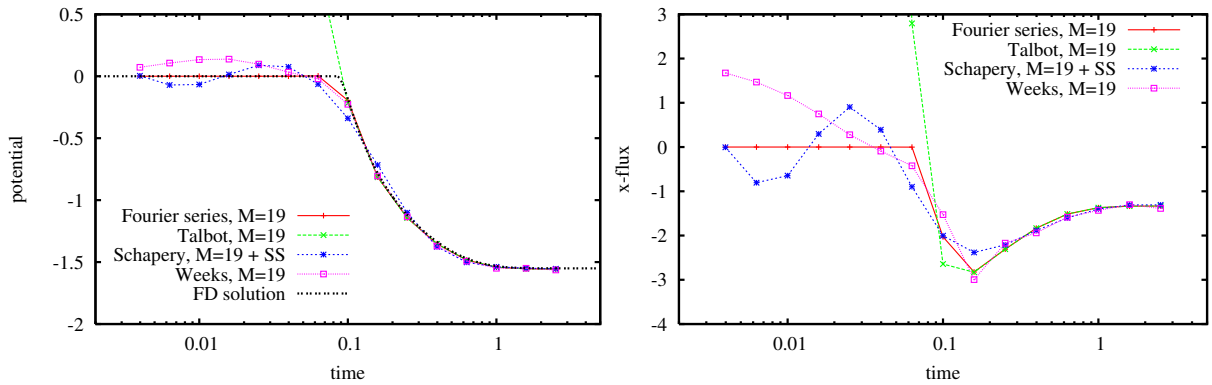


Fig. 7 Plots of potential and flux through time with four methods for $\bar{f}_t(p) = \exp(-0.08p)/p$, same p used across all t . 19 total $\bar{f}(p)$ evaluations are used by each method. Weeks' solution is undefined for $t < 0.08$.

250 4.4 Step-Change Boundary Condition for $\tau > 0$, same p

251 Finally, the same domain was simulated but with step-change boundary conditions at $\tau = 0.08$, or $\bar{f}_t(p) =$
 252 $\mathcal{L}(H(t - 0.08)) = e^{-0.08p}/p$, with singularities at the origin and $p = -\infty$. This function, and those derived
 253 from it (e.g., a pulse or a square wave) are difficult functions to invert accurately, because $f(t)$ is discontin-
 254 uous. Figures 7 and 8 show the Talbot method does not work for $t < \tau$ in double precision, since $\bar{f}_t(p)$ grows
 255 exponentially as $p \rightarrow -\infty$. The Weeks and Schapery methods do worse than the Fourier series approach
 256 (even with $N = 51$), but their parameters can be optimized further to improve these methods.

257 Although this step boundary condition could be implemented more accurately by shifting the results
 258 from the first example by $t = 0.08$, other step-derived time behaviors involving a pulse or square wave
 259 cannot be simplified in this way.

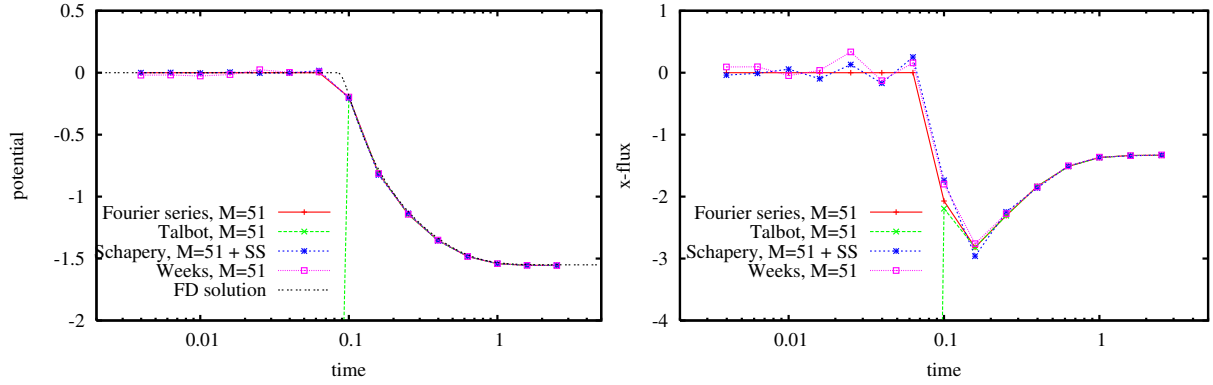


Fig. 8 Plots of potential and flux through time with four methods for $\bar{f}_t(p) = \exp(-0.08p)/p$, same p used across all t . 51 total $\bar{f}(p)$ evaluations are used by each method. Weeks' solution is undefined for $t < 0.08$.

Table 2 Numerical summary

Method	Number of Terms	Free Parameters	Implementation
Stehfest	$N \leq$ decimal precision	none	easiest
Schapery	depends on choice of p_j	p_j via trial & error	moderate
Weeks	$p \rightarrow i\infty$ slowly as N grows	κ & b (very sensitive to b)	moderate
fixed Talbot	$p \rightarrow -\infty$ quickly as N grows	$r = \frac{2M}{5t_{\max}}$ (automatic)	easy
Fourier series	$p \rightarrow i\infty$ slowly as N grows	$T = 2t_{\max}$ (automatic)	most difficult

260 4.5 Numerical Results Summary

261 Table 2 summarizes results from numerical testing with these four simple boundary condition time behav-
262 iors. The second column indicates what limit there is on the number of terms in the approximation and
263 therefore the accuracy of the method. The size of p required by the Weeks and Fourier series methods grow
264 much slower than those required by the fixed Talbot method. The third column indicates what paramete-
265 rs are needed to be tuned by the implementer to increase convergence of the method, and whether a
266 good choice is critical to the success of the method – an automatic method should not require searching
267 or optimizing parameters to obtain a robust solution. We define robustness as the ability of a solution to
268 remain useful, even when not at optimality. We prioritize a solution that is good enough and stable over
269 one that is excellent but catastrophically sensitive to parameter choice. The fourth column indicates the
270 ease of implementation in modern Fortran, Matlab, or NumPy. The methods could also be implemented in
271 a variable-precision environment like Mathematica or mpmath [Johansson(2011)], but this would further
272 require the BEM model be implemented in such an environment.

273 The modest success of the Schapery method is a bit surprising, given its simplicity and use of real p .
274 The results of the previous section were the product of many iterations of trial and error, this effort was
275 not included in the implementation effort. A better rule or parametrization of p_j might make this method
276 more widely useful.

277 The sensitivity of Weeks' method to the parameter choices was also surprising; similarly, the method
278 could have been improved after some optimization [Weideman(1999)], but Weeks' rule of thumb was used for
279 the parameters. One of the noted advantages of Weeks' method is the need to only compute optimal p once,
280 then any time can accurately be inverted [Kano et al(2005), Weideman(1999), Duffy(1993)]. When using the
281 simple rules-of-thumb for the the free parameters, this was not found to be the case. The generalized form
282 of Weeks' method can include information about behavior of $\bar{f}(p) \rightarrow \infty$ (related to behavior as $t \rightarrow 0$), but
283 this requires problem-specific knowledge.

284 The Fourier series method is more robust with respect to non-optimal p values, even though [Duffy(1993)]
285 cites this as a reason to use Weeks' method over the Fourier series approach.

286 5 Conclusions

287 Laplace-space numerical approaches to solve the diffusion equation have several viable alternative inverse
288 Laplace transform algorithms to choose from. Historically, most Laplace-space solutions to the diffusion
289 equation have used real-only methods (i.e., Gaver-Stehfest or Schapery). More robust methods require
290 complex arithmetic and $\bar{f}(p)$ evaluations, but have the benefits of:

- 291 1. handling a broader class of time behaviors (Fourier series method);
- 292 2. still being relatively simple to implement (fixed Talbot method);
- 293 3. only utilizing double-precision complex data types, which are handled natively by modern Fortran,
294 Matlab, or NumPy, and by common extensions in C++ (Fourier series and Weeks' methods).

295 Several practical recommendations are made regarding Laplace-space numerical modeling:

- 296 1. If many observations are needed across several time log cycles, large gains in efficiency can come from
297 inverting groups of times with a single $\bar{f}(p)$ vector (e.g., grouped by log cycle). This complicates the
298 implementation, but leads to much faster simulations.

- 299 2. If calculating $\bar{f}(p)$ is very expensive, and some numerical dispersion is allowable (not solving a wave
300 problem with sharp fronts), then the Fourier series method approach is most economical, and is auto-
301 matic and robust regarding free-parameter selection.
- 302 3. If only a single $\bar{f}_t(p)$ is needed, then it may be worthwhile to optimize free parameters needed by Weeks'
303 or Piessen's methods, or incorporate information about asymptotic $\bar{f}(p)$ behavior. Selection of optimum
304 b is far from automatic, and the Weeks method is not robust for non-optimal free parameters values.
- 305 4. If implementation time is a large factor, the fixed Talbot is quite simple to code and was automatic (no
306 need to select optimum parameters). The fixed Talbot may not work for non-zero step-time behavior
307 without extended precision.
- 308 5. If complex-valued function evaluations are not feasible (e.g., only real matrix or special function libraries
309 are available), the Schapery or Piessen's methods are capable of using the same p values to invert different
310 times, which the Gaver-Stehfest method cannot.
- 311 6. When appropriate, the strategy used by Schapery to expand the deviation from a reference state could
312 be incorporated as a strategy to improve other algorithms.

Acknowledgements The author thanks Professors Cho Lik Chan and Barry Ganapol from the Aerospace and Mechanical Engineering Department at the University of Arizona for initial inspiration and direction on this manuscript.

Sandia National Laboratories is a multi-program laboratory managed and operated by Sandia Corporation, a wholly owned subsidiary of Lockheed Martin Corporation, for the U.S. Department of Energy's National Nuclear Security Administration under contract DE-AC04-94AL85000.

References

- Abate and Valkó(2004). Abate J, Valkó P (2004) Multi-precision Laplace transform inversion. *International Journal for Numerical Methods in Engineering* 60:979–993, DOI 10.1002/nme.995
- Al-Shuaibi(2001). Al-Shuaibi A (2001) Inversion of the Laplace transform via Post-Widder formula. *Integral Transforms and Special Functions* 11(3):225–232, DOI 10.1080/10652460108819314
- Antia(2002). Antia H (2002) *Numerical Methods for Scientists and Engineers*, 2nd edn. Birkhäuser-Verlag
- Bailey et al(2002). Bailey DH, Hida Y, Li XS, Thompson B (2002) ARPREC: An arbitrary precision computation package. Tech. Rep. LBNL-53651, Lawrence Berkley National Lab
- Bakker and Kuhlman(2011). Bakker M, Kuhlman K (2011) Computational issues and applications of line-elements to model subsurface flow governed by the modified Helmholtz equation. *Advances in Water Resources* DOI 10.1016/j.advwatres.2011.02.008

- Barnhart and Illangasekare(2012). Barnhart KS, Illangasekare TH (2012) Automatic transport model data assimilation in Laplace space. *Water Resources Research* 48:W01510, DOI 10.1029/2011WR010955
- Bellman et al(1966). Bellman R, Kalaba RE, Lockett JA (1966) Numerical inversion of the Laplace transform: Applications to Biology, Economics, Engineering, and Physics. Elsevier
- Brebbia et al(1984). Brebbia C, Telles J, Wrobel L (1984) Boundary Element Techniques: Theory and Practice in Engineering. Springer-Verlag
- Cohen(2007). Cohen AM (2007) Numerical Methods for Laplace Transform Inversion. Springer
- Davies and Crann(2002). Davies A, Crann D (2002) Parallel Laplace transform methods for boundary element solutions to diffusion-type problems. *Electronic Journal of Boundary Elements BETEQ* 2001(2):231–238
- Davies(2005). Davies B (2005) Integral Transforms and their Applications, 3rd edn. Springer
- Davies and Martin(1979). Davies B, Martin B (1979) Numerical inversion of the Laplace transform: a survey and comparison of methods. *Journal of Computational Physics* 33:1–32, DOI 10.1016/0021-9991(79)90025-1
- de Hoog et al(1982). de Hoog F, Knight J, Stokes A (1982) An improved method for numerical inversion of Laplace transforms. *SIAM Journal of Scientific and Statistical Computing* 3:357–366, DOI 10.1137/0903022
- Duffy(1993). Duffy DG (1993) On the numerical inversion of Laplace transforms: Comparison of three new methods on characteristic problems from applications. *ACM Transactions on Mathematical Software* 19(3):333–359, DOI 10.1145/155743.155788
- Duffy(2004). Duffy DG (2004) Transform methods for solving partial differential equations. CRC Press
- Hantush(1960). Hantush M (1960) Modification of the theory of leaky aquifers. *Journal of Geophysical Research* 65(11):3713–3725, DOI 10.1029/JZ065i011p03713
- Johansson(2011). Johansson F (2011) mpmath: a Python library for arbitrary-precision floating-point arithmetic (version 0.17). <http://code.google.com/p/mpmath/>
- Kano et al(2005). Kano PO, Brio M, Moloney JV (2005) Application of the Weeks method for the numerical inversion of the Laplace transform to the matrix exponential. *Communications in Mathematical Sciences* 3(3):335–372
- Kuhlman and Neuman(2009). Kuhlman KL, Neuman SP (2009) Laplace-transform analytic-element method for transient porous-media flow. *Journal of Engineering Mathematics* 64(2):113–130, DOI 10.1007/s10665-008-9251-1
- Kythe(1995). Kythe PK (1995) An Introduction to Boundary Element Methods. CRC Press
- Lanczos(1988). Lanczos C (1988) Applied Analysis. Dover
- Liggett and Liu(1982). Liggett JA, Liu PL (1982) The Boundary Integral Equation Method for Porous Media Flow. Unwin Hyman
- Lyness and Giunta(1986). Lyness J, Giunta G (1986) A modification of the Weeks method for numerical inversion of the Laplace transform. *Mathematics of Computation* 47(175):313–322, DOI 10.2307/2008097
- Malama et al(2009). Malama B, Kuhlman K, Reil A (2009) Theory of transient streaming potentials associated with axial-symmetric flow in unconfined aquifers. *Geophysical Journal International* 179(2):990–1003, DOI 10.1111/j.1365-246X.2009.04336.x

- Mishra and Neuman(2010). Mishra PK, Neuman SP (2010) Improved forward and inverse analyses of saturated-unsaturated flow toward a well in a compressible unconfined aquifer. *Water Resources Research* 46(7):W07508, DOI 10.1029/2009WR008899
- Morales-Casique and Neuman(2009). Morales-Casique E, Neuman SP (2009) Laplace-transform finite element solution of nonlocal and localized stochastic moment equations of transport. *Communications in Computational Physics* 6(1):131–161
- Oliphant(2007). Oliphant TE (2007) Python for scientific computing. *Computing in Science and Engineering* 9(3):10–20, DOI 10.1109/MCSE.2007.58
- Piessens(1972). Piessens R (1972) A new numerical method for the inversion of the Laplace transform. *Journal of the Institute of Mathematics and its Applications* 10:185–192, DOI 10.1093/imamat/10.2.185
- Schapery(1962). Schapery R (1962) Approximate methods of transform inversion for visco-elastic stress analysis. In: *Proceedings of the Fourth US National Congress on Applied Mechanics*, vol 2, pp 1075–1085
- Stehfest(1970). Stehfest H (1970) Algorithm 368: numerical inversion of Laplace transforms. *Communications of the ACM* 13(1):47–49, DOI 10.1145/361953.361969
- Sternberg(1969). Sternberg Y (1969) Flow to wells in the presence of radial discontinuities. *Ground Water* 7(6):17–20, DOI 10.1111/j.1745-6584.1969.tb01666.x
- Sudicky and McLaren(1992). Sudicky E, McLaren R (1992) The Laplace transform Galerkin technique for large-scale simulation of mass transport in discretely fractured porous formations. *Water Resources Research* 28(2):499–514, DOI 10.1029/91WR02560
- Talbot(1979). Talbot A (1979) The accurate numerical inversion of Laplace transforms. *IMA Journal of Applied Mathematics* 23(1):97, DOI 10.1093/imamat/23.1.97
- Weeks(1966). Weeks W (1966) Numerical inversion of Laplace transforms using Laguerre functions. *Journal of the ACM* 13(3):419–429, DOI 10.1145/321341.321351
- Weideman(1999). Weideman J (1999) Algorithms for parameter selection in the Weeks method for inverting the Laplace transform. *SIAM Journal of Scientific Computing* 21(1):111–128, DOI 10.1137/S1064827596312432
- Widder(1941). Widder D (1941) *The Laplace Transform*. Princeton University Press